COMPDYN 2015
5th ECCOMAS Thematic Conference on
Computational Methods in Structural Dynamics and Earthquake Engineering
M. Papadrakakis, V. Papadopoulos, V. Plevris (eds.)
Crete Island, Greece, 25–27 May 2015

# SEISMIC RELIABILITY ASSESSMENT OF ROCKING BEHAVIOUR UNDER NEAR-FAULT EXCITATIONS

**Elias G. Dimitrakopoulos**[1], **and Themelina S. Paraskeva**[1]

[1] Hong Kong University of Science and Technology
Department of Civil and Environmental Engineering, Kowloon, Clear Water Bay, Hong Kong
e-mail: ilias@ust.hk

**Keywords:** Rocking, overturning risk, fragility curves, rocking bridges, earthquake engineering.

**Abstract.** *This paper assesses the seismic reliability of single degree of freedom rocking structures subjected to near-fault excitations within a probabilistic framework. In this context, it proposes a physically consistent and practically useful methodology to scale the rocking behavior for excitations of different intensity and predominant frequency. According to the assumptions of the proposed methodology the definition of both the Engineering Demand Parameter (EDP) and the corresponding limit states is rather straightforward, since when the rocking structure does not overturn it eventually returns to its original configuration without permanent deformation or damage. On the contrary, identifying appropriate intensity measure/s (IM/s) for rocking structures is far from trivial, longstanding challenge. Two groups of dimensionless-orientationless IMs are considered as candidate IMs: one giving the frequency ratio $\omega_g/p$ and one equivalent with the dimensionless slenderness $\alpha_g/(g\tan\alpha)$. Using four well-known strong ground motion parameters (the peak ground velocity, the peak ground acceleration, the predominant period of the pulse and the mean period of the CSGM) six different versions of IMs are examined. In addition, this study, introduces a more 'holistic' approach for the description of the rocking fragility using hybrid bivariate IMs. Analytical fragility curves (FCs) for slender, rigid rocking structures are obtained, using either univariate IM/s (conventional FCs) or bivariate IM/s (bivariate FCs). The study shows that while the use of a univariate IM is a simpler approach, it results in increased scatter. On the other hand, the more complex bivariate IM approach utilizes additional information and reduces uncertainty. Further, the study also unveils that when the rocking structure survives the excitation without overturning, the peak response follows a bi-planar distribution. Specifically, it brings forward the existence of critical peak ground motion acceleration, below and above which rocking response scales differently.*

# 1 INTRODUCTION

The present study focuses on slender rigid structures that exhibit rocking (without sliding) during seismic excitation. This work is part of a broader study [1-3] on the dynamics of rocking structures, which aims to examine the potential merits of rocking behavior as a seismic isolation technique for contemporary structures.

An essential characteristic of rocking dynamics is the negative stiffness that prevents the structure from resonance under constant frequency (e.g., harmonic) excitation [4]. However, the negative stiffness renders also rocking structures inherently unstable, and very sensitive to the characteristics of ground motion. Thus, rocking dynamics remain difficult to predict, especially if one considers the inherent uncertainty related to the specific characteristics of future ground motions. To deal with the non-predictability of rocking response several researchers adopted a probabilistic approach. Housner [5], in his 1963 paper, tackled the problem of rocking behavior also from a stochastic perspective, estimating the probability of overturning via an energy balance equation (see also [6]). Almost two decades later, researchers (e.g., [7]) showed that small changes in size, slenderness, or ground motion could cause drastic differentiation of the rocking response. This prompted the prediction of rocking overturning via probabilistic methods: Spanos and Koh [8] deployed a stochastic linearization technique, Cai et al. [9] assessed the reliability of a rigid block against toppling under nonstationary and nonwhite (random process) base excitations, and Shao and Tung [10] estimated the overturning probability of a rigid body subjected to real earthquake records. Kafle et al. [11] developed overturning fragility curves, for unrestrained blocks, based on physical and numerical experiments, while Roh and Cimellaro [12] and Deng et al. [13] offered fragility curves for frames with rocking columns [14] and bridges with rocking foundations, respectively.

Motivated by the growing interest in rocking, the present study acknowledges the need to tackle the non-predictability of the rocking response probabilistically. Its particular goal is to assess the seismic reliability of (negative stiffness) rocking structures to near-fault excitations. In this context, it integrates two different components: (i) a 'universal' description of rocking response from [2] and (ii) a probabilistic framework, from recent studies of Psycharis et al. [15] and Acikgoz and DeJong [16]. This work brings forward the different sensitivity of rocking response to excitations with low versus high amplitude. In addition it sheds light on the effect of the high-frequency stochastic component of the seismic excitation on rocking behavior and contributes towards improved, specialized intensity measures (*IMs*) for rocking.

# 2 PROBABILISTIC SEISMIC DEMAND ANALYSIS

## 2.1 Stochastic model for near-fault ground motions

For the assessment of the seismic reliability of a structure we can use either natural/historic records (e.g., [16]) or synthetic ground motions (e.g., [15]). In the present study, we employ a stochastic synthetic ground motion model [17-19]. First, we model the low-frequency (long period) and high-frequency components of the ground motion, independently (see Figure 1). Then, we superpose the two aforementioned components and generate the combined synthetic ground motions (CSGMs). For economy of space, we keep the presentation of the method (Section 2.1) short, as it is described in detail in [17-19] and references therein.

To model the low-frequency (coherent) pulse of the *CSGM*, we utilize the well-established Mavroeidis and Papageorgiou (M&P) [19] wavelet. Its velocity time-history expression is:

$$\dot{u}_p = \begin{cases} \frac{A}{2}\left[1+\cos\left(\frac{\omega_p}{\gamma_p}(t-t_0)\right)\right]\cos\left(\omega_p\left(t-t_0\right)+\upsilon_p\right), & t \in \left[t_0-\frac{\pi\gamma_p}{\omega_p}\ ,t_0+\frac{\pi\gamma_p}{\omega_p}\right] \\ 0 & otherwise \end{cases} \quad (1)$$

where $A$, $\omega_p$, $\upsilon_p$, $\gamma_p$ and $t_0$ describe the velocity amplitude of the envelope of the pulse, the angular frequency, the phase angle, the oscillatory character (i.e., number of half cycles), and the time shift to specify the epoch of the envelopes peak, respectively; $T_p$ ($=2\pi/\omega_p$) is the prevailing period of the pulse.

For every earthquake moment magnitude $M_w$ and epicentral distance from the fault $R_e$, the mean value of the velocity amplitude $V_p$ in centimeters/second and the corresponding mean value of the period $T_p$ in *s* are obtained from [20]:

$$\log(V_p) = -5.17 + 1.98M_w - 0.14M_w^2 - 0.10\log(R_e^2 + 0.562) \quad (2)$$

and

$$\log(T_p) = -2.87 + 0.47M_w \quad (3)$$

where *log* denotes the base *10* logarithm. Equation (2) holds for $M_w \le 7.0$; for higher values ($M_w > 7.0$), $M_w$ is taken as 7.0 [15]. The values of $M_w$ are in the range of 5.5 to 7.5 with a step of 0.5 (i.e., five values); the epicentral distance $R_e$ varies from 5 to 20 km with a step of 2.5 km (i.e., seven values) [15]. For each of the 35 $M_w$ scenarios, we generate 100 samples of the $V_p$, $T_p$, $\upsilon_p$ and $\gamma_p$ with the Latin hypercube sampling procedure [21]. Further, we assume that the logarithms of $V_p$ and $T_p$ follow a normal distribution with standard deviation equal to 0.16 and 0.18, respectively [15], and that $\gamma_p$ and $\upsilon_p$ follow also a normal distribution with mean values 1.93 and 1.83 and corresponding standard deviations 0.47 and 0.98, accordingly [22]. The distribution of $\gamma_p$ is left truncated to 1 [15]. Alternatively, the velocity pulse expression of Equation (2) can be utilized with the scaling laws of $T_p$ and $V_p$ proposed by Mavroeidis and Papageorgiou [19] and Halldorsson et al. [22], respectively. Note that the predominant periods estimated by [19] and [20] are not necessarily the same. In addition, the peak ground velocity (PGV) obtained from [20] has not the same value with the $V_p$ estimated by [22].

To model the high-frequency (*>0.1–0.2 Hz*) component (HFC) of the ground motions, we adopt the point source stochastic method of Boore [23]. The method uses a parametric description of the ground motion's radiation spectrum, which is a product of quantities that consider the effect of source, path, site, and instrument (or type) of motion. The duration of the ground motion is incorporated through an envelope function. Both the radiation spectrum and the duration of the ground motion depend on $M_w$ and $R_e$. The particular parameters used herein are taken from the Atkinson and Silva [24] study.

Finally, the CSGM is obtained by a superposition procedure of the two components (long-period and high frequency), which is described in detail in [17-19]. Overall, the model parameters consist of the seismological parameters $M_w$ and $R_e$, the additional parameters for the velocity pulse ($V_p$, $T_p$, $\upsilon_p$ and $\gamma_p$), and the white noise sequence [17, 18]. Figure 1 illustrates the two components, as well as the final (sample) CSGM. All simulations for this section are performed using MATLAB [21].

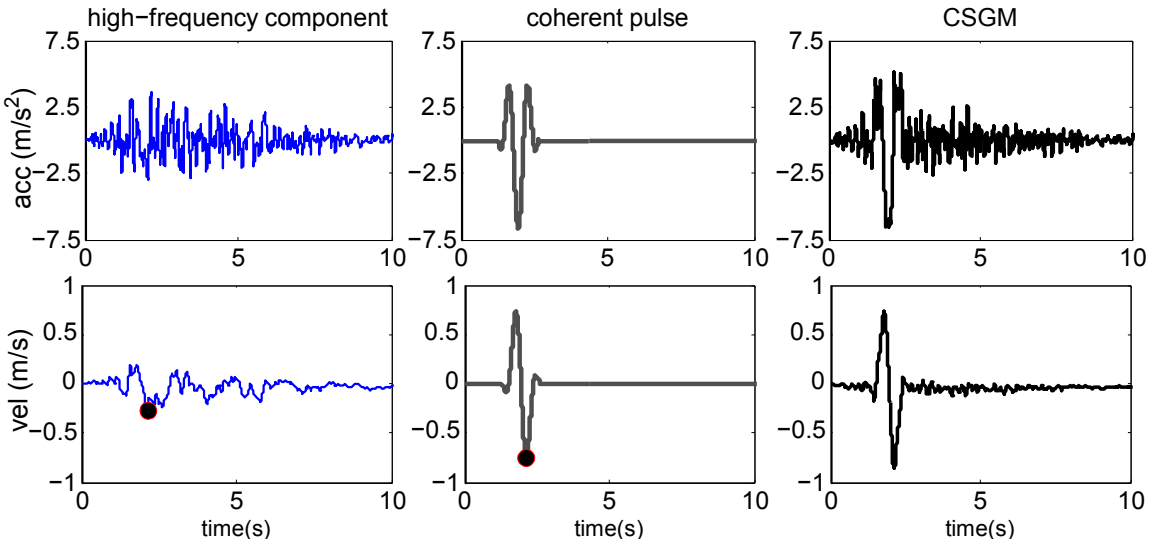


Figure 1: Sample of a CSGM: high frequency component (first column), pure/coherent pulse (second column). Acceleration time history (first row) and velocity time history (second row).

## 2.2 Structural/Seismic response analysis

The present study examines the seismic response of a rocking frame (see Figure 2). This is a single degree of freedom rocking structure. The equation of motion describing the pure rocking behavior of this structure subjected to a horizontal ground motion with acceleration time history $\ddot{u}_g(t)$ [25] is:

$$\ddot{\theta} = -p^2\left(\sin\left[\alpha\,\mathrm{sgn}(\theta)-\theta\right]+\frac{\ddot{u}_g}{g}\cos\left[\alpha\,\mathrm{sgn}(\theta)-\theta\right]\right) \tag{4}$$

where *sgn()* is the (standard) sign function; $\alpha$ is the slenderness angle; $g$ is the acceleration of gravity; and $p$ ($=p_f$) is the rocking frequency parameter for the rocking frame [25], given as:

$$p_f = \frac{1+2\gamma}{1+3\gamma}\sqrt{\frac{3g}{4R_o}} \tag{5}$$

where, $\gamma$ is the beam-to-columns mass ratio; and $R_o$ is the semi-diagonal. If sliding is restricted a sufficiently slender frame uplifts and commences rocking once the ground acceleration exceeds a minimum magnitude:

$$\ddot{u}_{g,\min} = \alpha_{g,\min} = g\tan(\alpha) \tag{6}$$

Impact takes place when the structure returns to its initial position ($\theta$=0). Then, the pivot point changes, and the rotation switches sign. To treat impact is with a coefficient of restitution $\eta$, which is taken as the ratio of the post-impact ($\dot{\theta}^+$)and pre-impact ($\dot{\theta}^-$) angular velocities. The value of $\eta$ is material and application dependent (e.g., [1, 2] and references therein) and, therefore, is considered as an additional, independent, governing parameter of the rocking problem. In the present study, we use a coefficient of restitution equal to $\eta$=0.92. The rocking response is determined numerically solving the nonlinear equations of motion (4) in MATLAB [21].

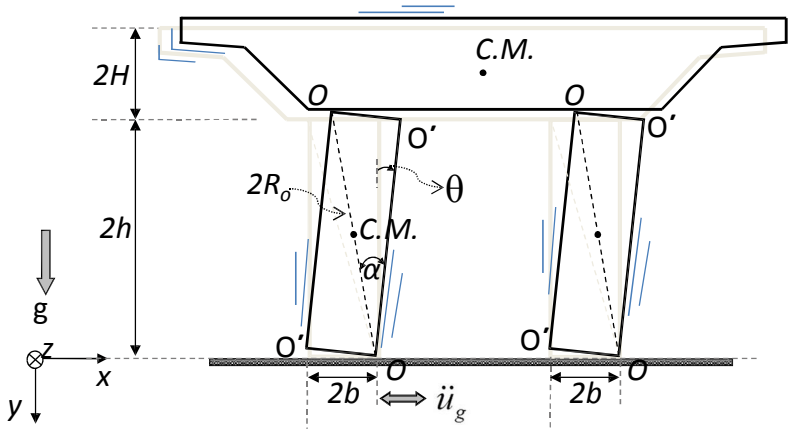


Figure 2: Adopted rocking structure: the single degree of freedom rocking frame.

### 2.3 Engineering demand parameters and limit states

The definition of appropriate engineering demand parameters (*EDPs*) and limit states (*LS*), for rocking structures, is straightforward, considering the assumptions of the present study. We adopt as *EDP* the absolute peak rocking rotation $|\theta_{max}|$ scaled with respect to the slenderness, $a$:

$$EDP = \frac{|\theta_{max}|}{\alpha} \tag{7}$$

The dimensionless *EDP* of Equation (7) has a straightforward physical meaning: values larger than zero imply that the structure commences rocking, whereas high values (e.g., $EDP > 1.5$) indicate overturning due to rocking. Accordingly, we define two pertinent performance levels as an upper and a lower limit to assess the response of a rocking structure: the lower limit ($LS_l$) marks the initiation of rocking and it is equal to zero; the upper limit ($LS_{up}$) corresponds to overturning due to rocking. Overturning occurs, when the system becomes dynamically unstable, in which case the response tends to numerically infinite values. Thus, the threshold of $LS_{up}$ does not correspond to a particular rotation value (e.g., $EDP = 1.5$), but rather at $EDP \rightarrow \infty$. Intermediate limit states $LS_1, LS_2, ..., LS_n$ can also be defined to indicate observable rocking during seismic response. The values of these limit states are based on engineering judgment to express the level of marginal/limited rocking action that is usually targeted in rocking applications without the substantial danger of overturning. In this context, we define three limit states equal to 0.10, 0.25 and 0.50 to indicate a structure that exhibits rocking without overturning, for different levels of observable damages due to contact (see Figure 10 later on).

Figure 3 plots the *EDP* values of all nonlinear dynamic response analyses (in total 3500) versus the peak ground velocity *PGV* (Figure 3 (b)) (or $V_p$ in the case of pure pulse ground motions, in Figure 3 (a)) and the prevailing period $T_p$ of the pulse. Figure 3 concerns a rocking bridge frame/bent [25] (as shown in Figure 2), with frequency parameter $p = p_f = 1.0$ rad/s and slenderness $a$=0.149 rad. The structure is subjected to two suites of ground motions: (a) pure M&P pulses (Figure 3(a) top panel), and (b) CSGMs (Figure 3(b) bottom panel). The results are divided in three groups: (i) the 'non-rocking' simulations (crosses), when the peak ground acceleration is less than the minimum acceleration that initiates rocking (Eq.(6)) and hence the structure remains at rest; (ii) the 'safe-rocking' simulations (hollow circles), when the structure commences rocking and does not overturn, and (iii) the 'rocking-overturning'

simulations (solid circles). Recall that a rocking structure becomes statically unstable after $EDP \geqslant 1.0$, because the highly nonlinear nature of rocking dynamics overturning does not necessarily occur when $EDP \geqslant 1.0$. On the contrary, a rocking structure might exhibit significantly higher rotations $\theta_{max}$ than $\alpha$ without overturning [3], a behavior counter to the common quasi-static viewpoint of seismic response.

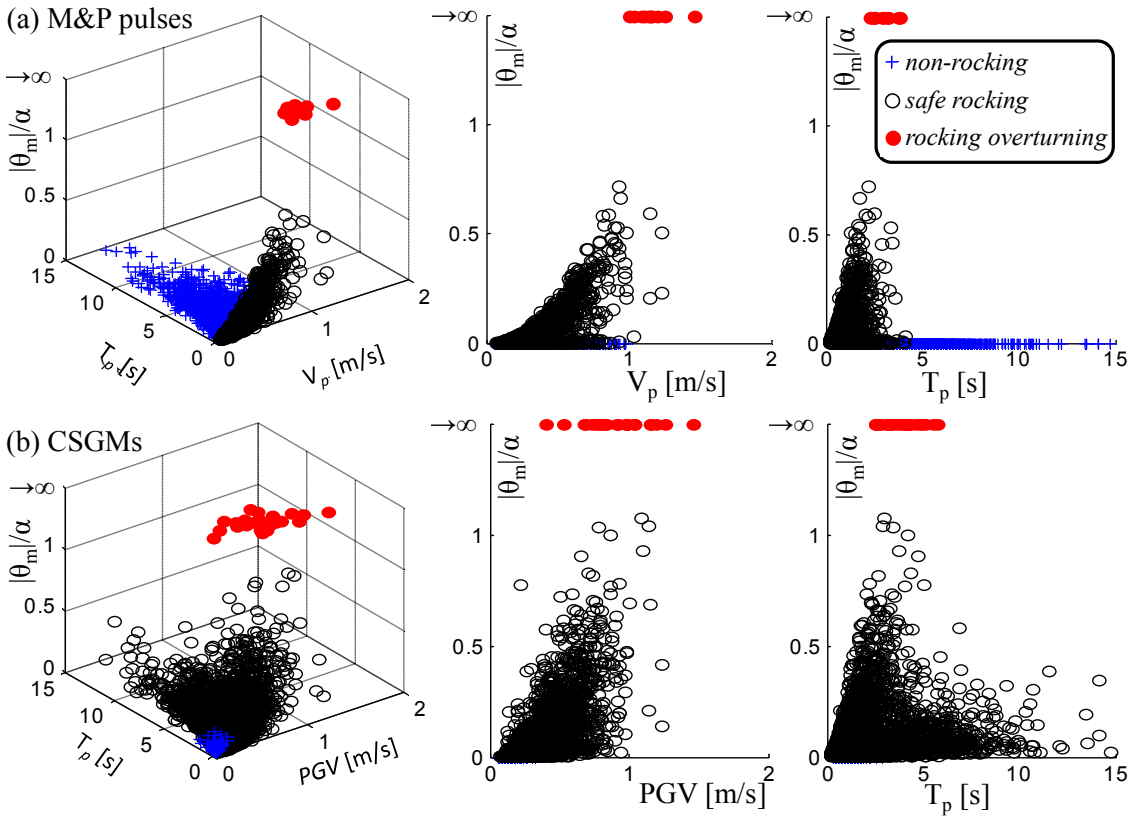


Figure 3: Seismic response analyses of a rocking frame with $p=1.0$ *rad/s* and $\alpha=0.20$ *rad*.

The results of Figure 3 verify the sensitivity of rocking structures to the characteristics of the ground motion and bring forward the influence of the stochastic HFC in the excitation. Note the virtual straight line on the $V_p$-$T_p$ plane that separates the 'non-rocking' from the rocking simulations in Figure 3 (top left). The slope of this separating limit line on the $T_p$-$V_p$ plane, corresponds to the minimum ground acceleration (Equation (6)) that triggers (uplifting and) rocking. However, when the stochastic HFC is included in the excitation, this limit line disappears (Figure 3, bottom left), the number of 'non-rocking' simulations is drastically reduced, and rocking response becomes significantly more probable. This is because of the numerous CSGMs for which the presence of the HFC triggers rocking, whereas the (low acceleration M&P) pulse alone would not. Consequently, this introduces observable noise in the results (Figure 3, bottom right), and the response becomes less ordered. Figure 3 verifies also that rocking is sensitive to more than one strong ground motion parameters. Overturning occurs as both $PGV$ and $T_p$ increase, without though a distinguishable pattern.

### 2.4 Physically similar ('universal') rocking behavior

In this section we propose a physically consistent method to scale the rocking behavior for excitations of different intensities and predominant frequencies. According to this concept, we generate normalized fragility curves, indifferent to the size and the frequency of the rocking structure or the amplitude and the predominant frequency of the near-fault ground motion.

For a given ground motion with a specific waveform (i.e., a specific acceleration time-history shape), for example, the CSGM excitation of Figure 1, the (acceleration) amplitude $\alpha_g = PGA$ and the frequency $\omega_g = 2\pi/T_p$ characterize the length and time scale of the waveform, respectively [26]. Then, the response (e.g., the absolute peak rocking rotation) can be written as a function of the general form:

$$|\theta_{\max}| = f\left(\alpha, p, \omega_g, \frac{\alpha_g}{g}, \eta\right) \tag{8}$$

Equation (8) contains six characteristic variables that involve only one reference dimension, time [T]. The six variables can be grouped into a reduced number of independent dimensionless Π-products according to Buckingham's Π theorem [27], which can be further reduced to a group of dimensionless- orientantionless products, according to the theory of orientational analysis [2, 28] as:

$$\frac{|\theta_{\max}|}{\alpha} = \phi\left(\frac{\omega_g}{p}, \frac{\alpha_g}{g\alpha}, \eta\right) \tag{9}$$

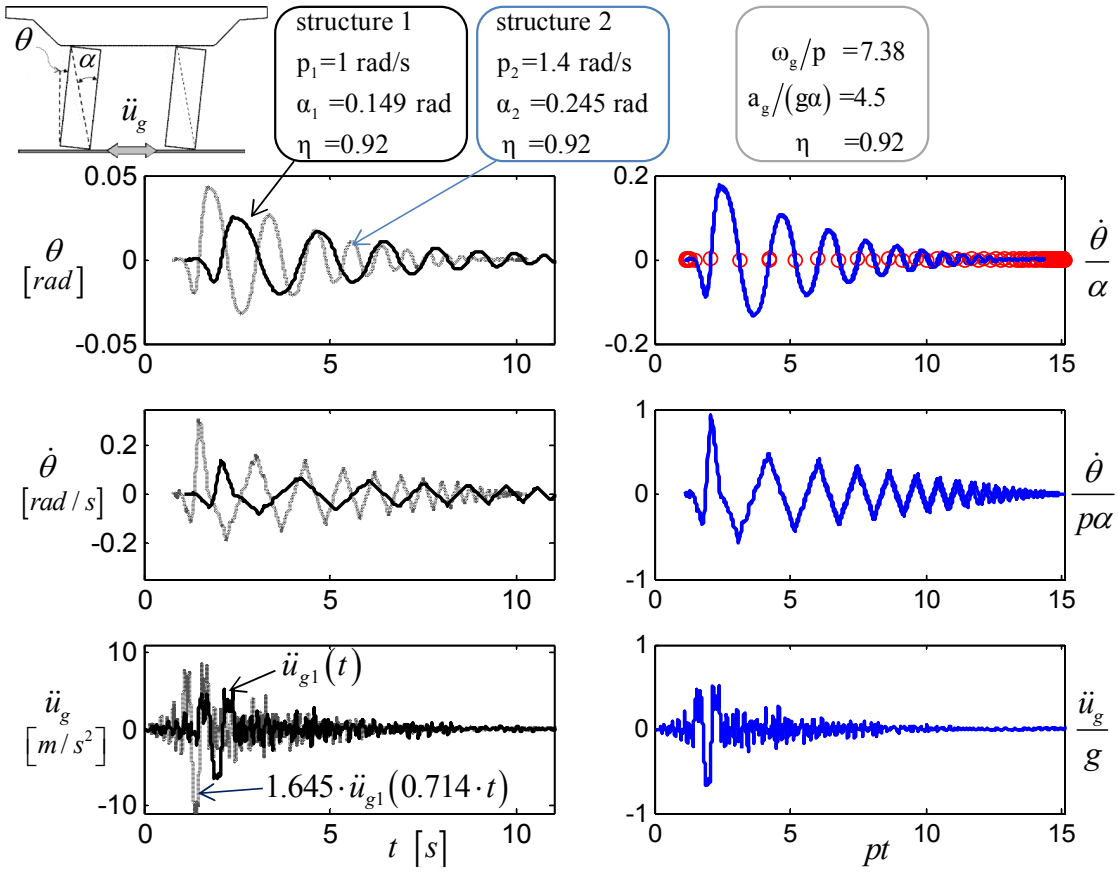


Figure 4: Seismic physically similar rocking response for frame-structures subjected to different CSGMs.

The products of Equation (9) yield an exact representation of the rocking response when the slenderness angle $\alpha$ is small [2]. If $\alpha$ is not small, it should be included explicitly as an additional independent group [2].This study focuses solely on the case of small $\alpha$ (slender rocking structures).

Figure 4 (left) illustrates the time-history response of two different rocking structures, subjected to two CSGM excitations of different amplitude and frequency, but the same waveform (of Figure 1), The two structures differ both in size ($p$) and in shape ($\alpha$). However, when the associated dimensionless–orientationless products of Equation (9) take the same values, the response curves of the two different structures are identical (Figure 4 (right)). This *physical similarity* (or self-similarity in [45]) is a special type of symmetry of unique importance for nonlinear phenomena. The dimensionless - orientantionless groups of Equation (9) unveil what matters in rocking response, for example, not the frequency parameter, $p$ or slenderness $\alpha$ but the frequency ratio $\omega_g/p$, or the dimensionless-orientationless slenderness $a_g/(g\alpha)$.

### 2.5 Intensity measures (*IMs*)

Following the proposed dimensionless–orientationless products of Equation (9), we select *IMs* similar to that in [29] for sliding objects. According to Equation (9), there are two groups that could be considered as candidate *IMs*: the frequency ratio $\omega_p/p$ and the dimensionless slenderness $\alpha_g/(g\tan\alpha)$. We examine four common strong ground motion parameters that could be used as $\alpha_g$ or $\omega_g$ accordingly: the peak ground velocity $PGV$ (= $V_p$ for pulse excitations), the peak ground acceleration PGA, the predominant period $T_p$ of the pulse, and the mean period of the CSGM $T_m$ (see [26] and references therein). Using the four well-known strong ground motion parameters, we construct the following alternative versions of the two groups $\omega_p/p$ and $\alpha_g/(g\tan\alpha)$:

$$IM_1 = \frac{\omega_p}{p}, IM_2 = \frac{\omega_m}{p}, IM_3 = \frac{PGA}{pPGV}$$
$$IM_4 = \frac{PGA}{g\tan\alpha}, IM_5 = \frac{pPGV}{g\tan\alpha}, IM_6 = \frac{\omega_m PGV}{g\tan\alpha} \quad (10)$$

where $\omega_p = 2\pi / T_p$ and $\omega_m = 2\pi / T_m$; *IMs* $IM_1$ to $IM_3$ reconstruct the frequency ratio ($\omega_p / p$ of Equation (9)), whereas $IM_4$ to $IM_6$ are alternative dimensionless slenderness ($\alpha_g/(g\tan\alpha)$ of Equation (9)) groups. In the following, we refer to the former as 'frequency ratio' *IMs* and to the latter as 'dimensionless slenderness' *IMs*.

## 3 FRAGILITY ANALYSIS

In general, fragility (or vulnerability) analysis is the estimation of the conditional probability $P_f$ that an *EDP(=D)*, will exceed a certain capacity limit C(= *c)*, given an *IM* value:

$$P_f = P\left(D > C = c \mid IM\right) \quad (11)$$

Figure 5 illustrates the probability tree diagram that describes the rocking problem and facilitates the calculation of the conditional probability $P_{f|r}$, that the *EDP* of a structure will exceed a certain (capacity) threshold, given an *IM* value and given that the structure is rocking. $P_{nr}$ is the probability that the structure will remain resting on the ground (non-rocking response; Figure 5) during the earthquake excitation; $P_{ro}$ is the probability that the rocking structure overturns. In general, the probability $P_{f|r}$ is derived by the union of two likelihoods (Figure 5): (a) the probability that the structure commences rocking and overturns, and (b) the

rocking structure does not overturn, but during its rocking response, the *EDP* exceeds the capacity limit c. Thus, Equation (11) becomes [15]

$$P_{f|r} = P_{ro} + (1 - P_{ro}) P_{ex}(D > C \mid IM) \tag{12}$$

The overturning probability, $P_{ro}$ (in Figure 5), can be estimated as in [15], from the ratio of the number of simulations (response analyses) that result to rocking overturning to the total number of the simulations. An alternative solution for the estimation of probability $P_{ro}$ is [30], to adopt a maximum likelihood approach ($P_{nr}$, in Figure 5). The present study, focuses on the calculation of the conditional probability $P_{ex}$ of Equation (12), in which the *EDP* of a rocking structure will exceed a capacity limit, $C=c$, given an *IM* value without overturning.

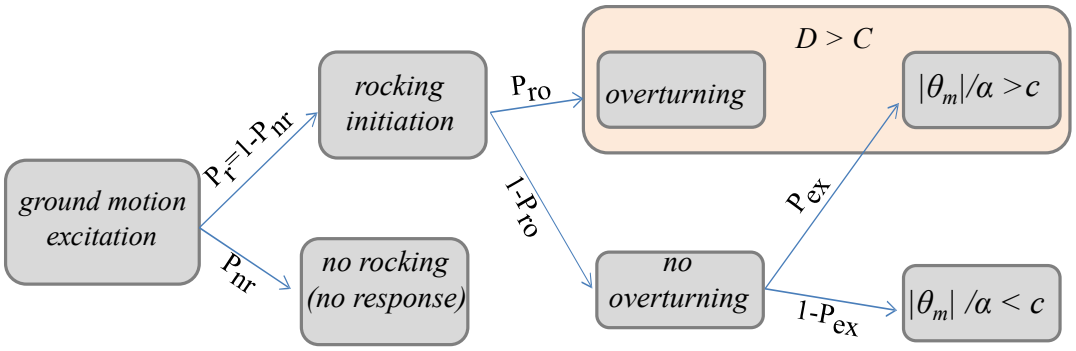


Figure 5: Probability tree diagram for the rocking problem.

### 3.1 Probability of limit state exceedance during 'safe rocking'.

In this section we present the calculation of the conditional probability $P_{ex}$ (see Figure 5 and Equation (11)) that a rocking structure exceeds a performance/capacity limit C(=*c*), without the occurrence of overturning ('safe rocking') under a ground motion with $IM = x$. The calculation procedure is based on two typical assumptions.

Firstly, that both the capacity $C$ and the demand $D$, are random variables following lognormal distributions. Then, $P_{ex}$ is:

$$P_{ex} = P_{ex}(D > C \mid IM = x) = \Phi\left(\frac{\ln x - \mu}{\beta_{D|IM}}\right) \tag{13}$$

where $\Phi(\ )$ is the standard normal cumulative distribution function; $\mu$ is the median value of the structural demand as a function of *IM* and $\beta_{D|IM}$ is the dispersion (or logarithmic standard deviation) of the demand conditioned on the *IM* [31].

The second typical assumption ([32]) is that the median demand $D_m$ and the *IM* are related through the function:

$$D_m = \alpha (IM)^b \tag{14}$$

Conveniently, the assumed function (Eq. (14)) becomes a straight line on the ln$D_m$ vs ln*IM* plane:

$$\ln(D_m) = \ln(\alpha) + b \ln(IM) \tag{15}$$

which enables the estimation of parameters $\alpha$ and $b$ by means of linear regression analysis.

Figure 6 presents sample results of the linear regression analyses considering solely rocking without the overturning ('safe rocking' cases of Figure 3). The regression analyses show a significant dispersion in the response for both pure pulse excitations (Figure 6 (a)), as well as, CSGMs (Figure 6 (b)). Regardless which of the *IMs* performs best compared with the others, none of the examined *IMs* shows a strong effect on the response. To some extent, this failure of the well-known strong ground motion parameters (e.g., *PGV, PGA, PGA/PGV*) to predict rocking response should be attributed to the negative stiffness mechanism and further to the lack of resonance of rocking structures under constant frequency ground motions [4].

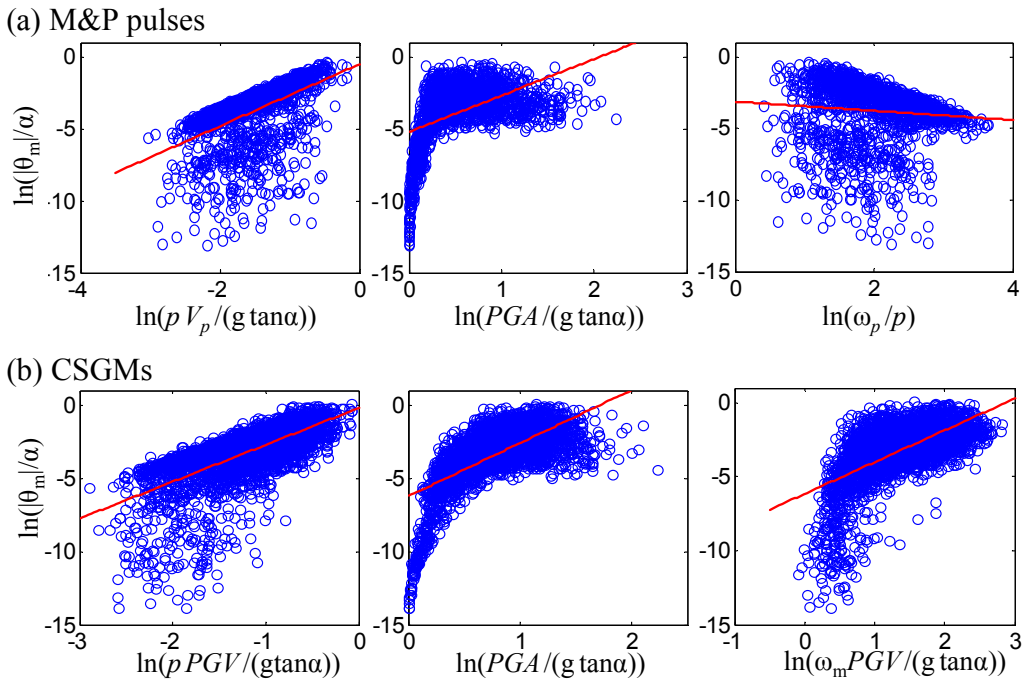


Figure 6: Sample results of the linear-regression analyses for (a) pure M&P pulse excitations and (b) CSGMs.

### 3.2 Proposed bivariate *IMs*

Alternatively, this section, examines the use of bivariate *IMs*, instead of univariate *IMs*, to capture the rocking response of a structure subjected to seismic (synthetic) excitations [31].

Figures 7 (a) and 8 (a) present a three-dimensional view, $\ln(|\theta_{max}|/\alpha) - \ln V_p - \ln T_p$, of the same 'safe-rocking' simulations (of Figure 3) for pure M&P pulse ground motions and for CSGMs, respectively. In the same Figures, the results are also plotted in the three two-dimensional viewpoints of the 3D plane: (i) a $\ln V_p$-$\ln T_p$ (Figures 7 (b) and 8 (b)), (ii) a $\ln(|\theta_{max}|/\alpha) - \ln V_p$ (Figures 7 (c) and 8 (c)), and (iii) a $\ln(|\theta_{max}|/\alpha) - \ln T_p$ view slice (Figures 7 (d) and 8 (d)). If viewed from the proper viewpoint (compare Figures 7 (a) and 8 (a) with Figures 9(a) and (b), respectively), remarkable order emerges: The response points lie consistently on two distinct planes; a trend hidden in the two-dimensional representations of the same results (e.g., Figure 6). The existence of the two distinct planes unveils that rocking response scales differently for low intensity, versus high intensity, excitations. In particular, rocking is more sensitive to low amplitude excitations, meaning that even slight variations of the excitation characteristics have a strong effect on the peak rocking response. Figure 9 illustrates alternative three-dimensional plots from different viewing angles of the same results of Figures 7 (a) and 8 (a), respectively.

In general, the equation of a plane in a three-dimensional ($\ln(|\theta_{max}|/\alpha)$ – $\ln IM_x$ – $\ln IM_y$) space is given as:

$$\ln(D_m) = b_1 \ln(IM_x) + b_2 \ln(IM_y) + \ln(\alpha) \tag{16}$$

which suggests that the mean demand is given by a bivariate (vector-valued) intensity measure $\hat{IM} = (IM_x, IM_y)$ as

$$D_m = \alpha \left( IM_x^{b_1} IM_y^{b_2} \right) \tag{17}$$

where $IM_x$ and $IM_y$ are two appropriate (scalar) *IMs*, and α, $b_1$, $b_2$ are coefficients calculated using multi-linear regression analysis [50]. For $IM_x$ and $IM_y$, we adopt the dimensionless slenderness $IM_4$ , and the frequency ratio $IM_3$ from Eq. (10), respectively, based on [30].

| Excitation | 1.00<PGA/(g tanα) <1.30 | | | | PGA/(g tanα)≥1.30 | | | |
|---|---|---|---|---|---|---|---|---|
| | α | $b_1$ | $b_2$ | ($R^2$) | α | $b_1$ | $b_2$ | ($R^2$) |
| M&Ps | 0.001 | 29.40 | -1.994 | (0.915) | 1.490 | 1.574 | -2.004 | (0.896) |
| CSGMs | 6.02e-6 | 28.31 | -0.236 | (0.737) | 0.104 | 2.640 | -1.436 | (0.557) |

Table 1: The fitted planar distributions for the response analyses of Figure 3.

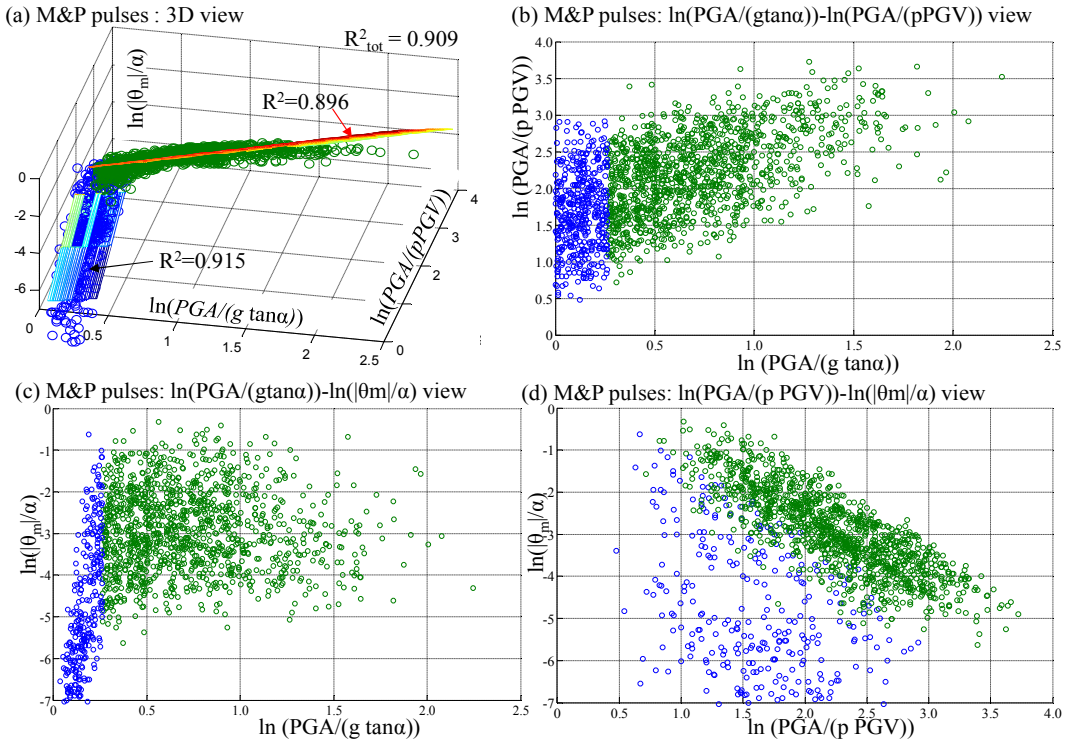


Figure 7: Plots of 'safe-rocking' results ( same as Figure 6(a))for M&P pulses excitations in: (a) a 3D plane; (b) a $\ln V_p$-$\ln T_p$ , (c) a $\ln(|\theta_{max}|/\alpha)$ – $\ln V_p$, and (d) a $\ln(|\theta_{max}|/\alpha)$ – $\ln T_p$ views.

The transition between the two planes takes place at a constant acceleration boundary (Figures 7 and 8). The estimation of the transition limit can be made with iterative multi-linear regression analyses that minimize the dispersion of both planes of Figures 7 and 8 simultaneously (e.g., through the coefficients of determination $R^2$). The 'low' (e.g., $PGA < 1.30\ \alpha_{g,min}$)

and the 'high' (e.g., $PGA > 1.30\ \alpha_{g,min}$) amplitudes are then defined according to the minimum rocking acceleration $\alpha_{g,min}=g\tan\alpha$.

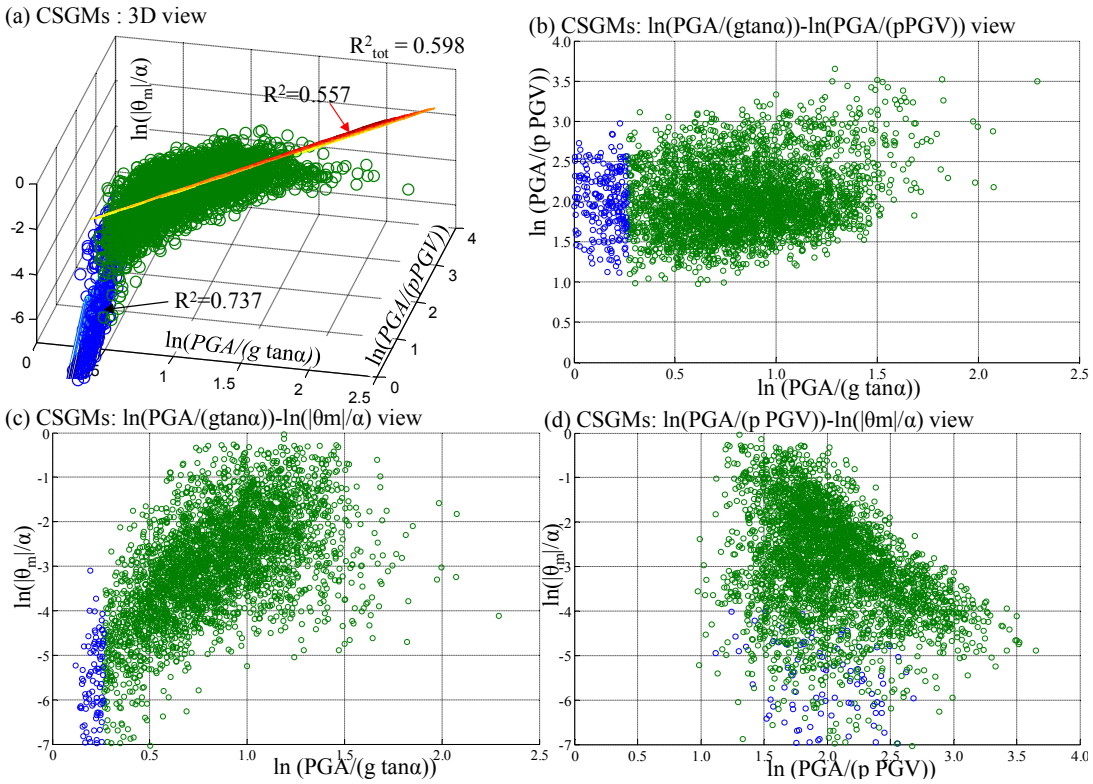


Figure 8: Plots of 'safe-rocking' results (same as Figure 6(b)) for the combined synthetic ground motions for different views: (a) a 3D view; (b) a $\ln V_p$-$\ln T_p$ , (c) a $\ln(|\theta_{max}|/\alpha) - \ln V_p$, and (d) a $\ln(|\theta_{max}|/\alpha) - \ln T_p$ views

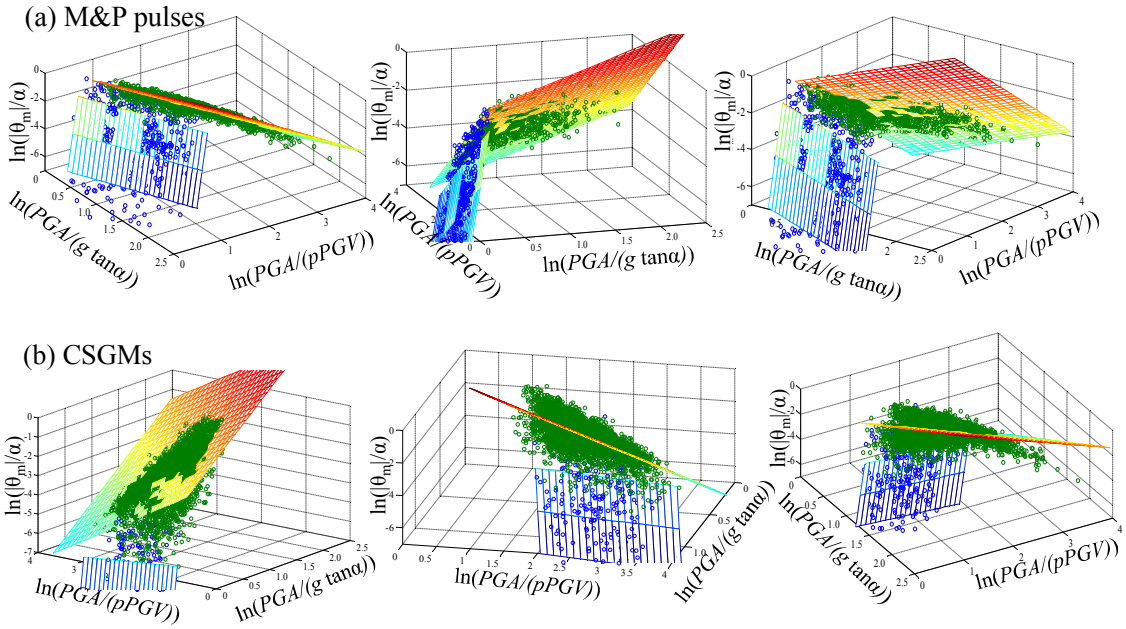


Figure 9: Alternative 3D views from other viewing angles of: (a) Figure 7(a) plot, and (b) Figure 8(a) plot.

In Table 1 are listed all the regression parameters $\alpha$, $b_1$, $b_2$, and the coefficient of correlation $R^2$ (i.e. the fitted planar distributions) when the structure (e.g., the rocking frame with $p$= *1.0 rad/s* and $\alpha$= *0.149 rad*) is subjected either to pure (M&P) pulses or CSGMs.

## 4 PROPOSED 'UNIVERSAL' FRAGILITY CURVES

In this section, we estimate the probability of a limit state threshold ($LS_i$) being exceeded during 'safe rocking' $P_{ex}$. The fragility curves of $P_{ex}$ can be generated using either a univariate or a bivariate *IM*. The use of a univariate *IM* is a simpler approach, but (as shown late in Figure 10) it results in increased scatter. Moreover, the more complex bivariate *IM* approach reduces drastically the uncertainty (Figure 10), but it requires more information about the frequency content of the excitation.

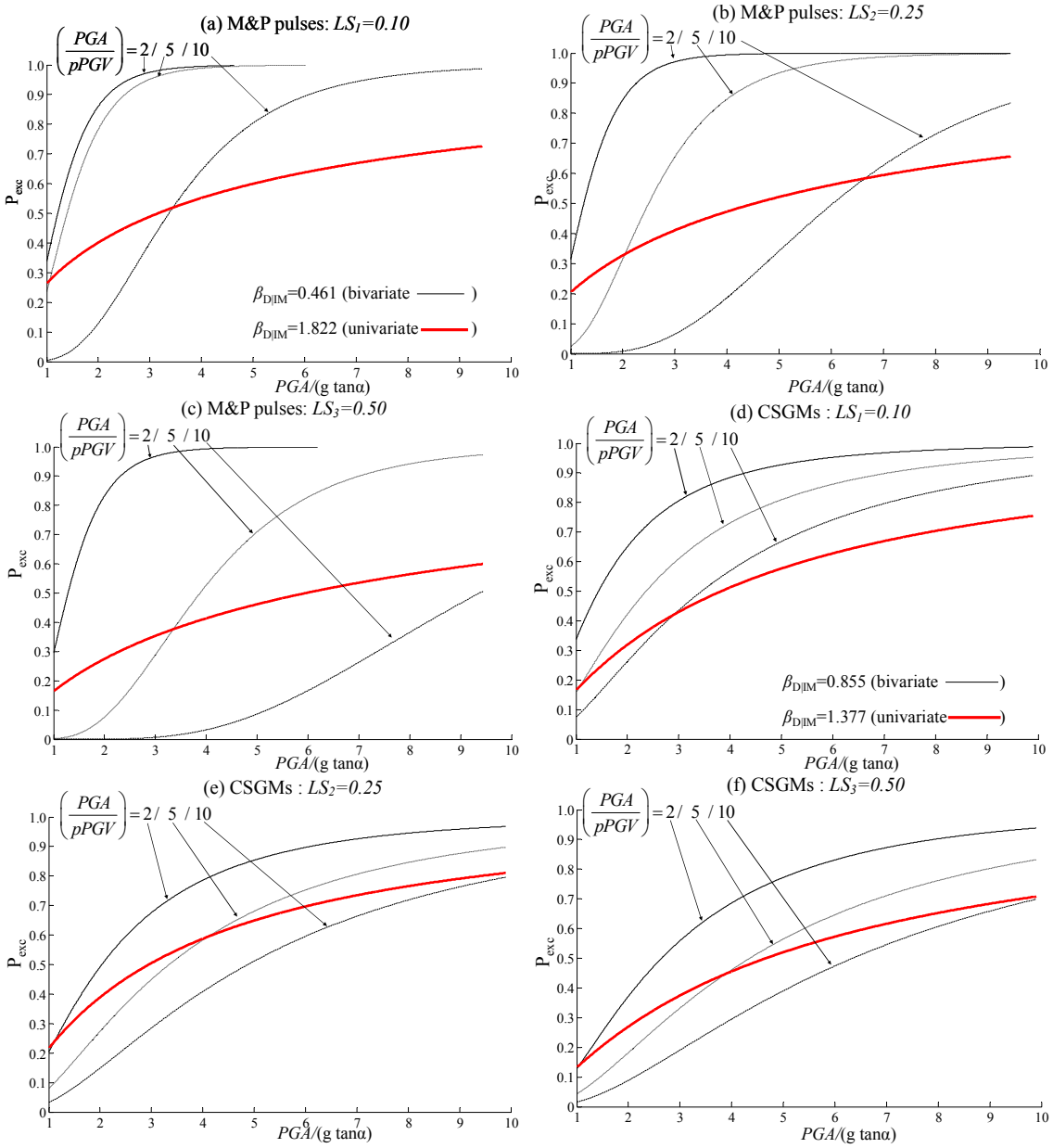


Figure 10: Comparison of bivariate with univariate $P_{ex}$ fragility curves for different *PGA/( pPGV)* values.

Figure 10 plots $P_{ex}$ fragility curves of different limit states using *pPGV/(g tana)* as the univariate *IM* and the pair of *IMs*, (*PGA/(gtana)*, *pPGV/PGA*) as a bivariate *IM*. The fragility curves of Figures 10 (a) to (c) are obtained for M&P pulse excitations (Figure 3(a)), while the fragility curves of Figures 10 (d) to (f) are obtained for CSGMs (Figure 3b). The limit states we adopt herein are: $LS_1=0.10$ (Figures 10 (a) and 10 (d)), $LS_2=0.25$ ((Figures 10 (b) and 10 (e)), and $LS_3=0.50$ ((Figures 10 (c) and 10 (f)). These values are based on engineering judgment, and they express an amplitude of rocking action raging from marginal up to extensive rocking. In particular, $LS_1$ indicates a rocking structure that may have minor and local damage due to contact. Accordingly, $LS_3$ corresponds to extensive local damages, while $LS_2$ demonstrates an intermediate level of observable local damages on the rocking structure. Figure 10, compares the univariate *FC* with bivariate *FCs* for given *PGA/PGV* values. As the *PGA/PGV* ratio increases, the fragility of the rocking structure (Figure 10) decreases a well-known trait of rocking behavior that the univariate *FCs* neglect. In addition, the univariate *FC* is substantially flatter than the bivariate *FCs*, which indicates higher uncertainty.

## 5 CONCLUSIONS

This paper offers analytical *FCs* for slender, rigid structures rocking under (synthetic) near-fault ground motions. The proposed *FCs* can be generated by either univariate (conventional) *IM* or bivariate *IM/s*. The study shows that the bivariate *FCs* offer a superior estimation of the fragility, compared with the conventional univariate *FCs*. In this context, the study proposes a group of various dimensionless–orientationless *IMs* that offer a normalized (approximately 'universal') description of rocking, indifferent to the characteristics of the structure or to the $a_g$ and $\omega_g$ of the (near-fault) ground excitations. Importantly, the paper unveils that rocking response without overturning follows a biplanar distribution with respect to the frequency ratio and the scaled acceleration amplitude of the ground motion. In particular, the paper brings forward the existence of a critical peak ground acceleration, below and above which, rocking response scales differently. This observation is stronger for pure pulse ground motions.

## REFERENCES

[1] M.J. DeJong, E.G. Dimitrakopoulos, Dynamically equivalent rocking structures. *Earthquake Engineering & Structural Dynamics,* **43**, 1543-63, 2014.

[2] E.G . Dimitrakopoulos, M.J. DeJong, Revisiting the rocking block: closed-form solutions and similarity laws. *Proceedings of the Royal Society A: Mathematical, Physical and Engineering Science*, **468**, 2294-318, 2014.

[3] E.G. Dimitrakopoulos, A.I. Giouvanidis A.I., Seismic Response Analysis of the Planar Rocking Frame. *Journal of Engineering Mechanics(ASCE)*, accepted for publication, 26/1/2015

[4] M.J. DeJong, Amplification of rocking due to horizontal ground motion. *Earthquake Spectra*, **28**:1405-21, 2012.

[5] G.W. Housner, The behavior of inverted pendulum structures during earthquakes. *Bulletin of the seismological society of America*, **53**, 403-17, 1963.

[6] K. Aydin, C. Tung, Energy balance equation for estimating overturning potential of an unanchored rocking body subjected to earthquake excitation. *Earthquake Spectra*, **17**, 209-20, 2001.

[7] C.S. Yim, A.K. Chopra, J. Penzien, Rocking response of rigid blocks to earthquakes. *Earthquake Engineering & Structural Dynamics*, **8**, 565-87, 1980.

[8] P.D. Spanos, A.S. Koh, Analysis of block random rocking. *Soil Dynamics and Earthquake Engineering*, **5**, 178-83, 1986.

[9] G. Cai, J. Yu, Y. Lin, Toppling of rigid block under evolutionary random base excitations. *Journal of Engineering Mechanics*, **121**, 924-9, 1995.

[10] Y. Shao, C. Tung, Seismic response of unanchored bodies. *Earthquake Spectra*, **15**, 523-36, 1999.

[11] B. Kafle, N.T. Lam, E.F. Gad, J. Wilson, Displacement controlled rocking behaviour of rigid objects. *Earthquake Engineering & Structural Dynamics*, **40**, 1653-69, 2011.

[12] H. Roh, G.P. Cimellaro, Seismic fragility evaluation of RC frame structures retrofitted with controlled concrete rocking column and damping technique. *Journal of Earthquake Engineering*, **15**,1069-82, 2011.

[13] L. Deng, B.L. Kutter, S.K. Kunnath, Probabilistic seismic performance of rocking-foundation and hinging-column bridges. *Earthquake Spectra*, 28:1423-46, 2012.

[14] H. Roh, A.M. Reinhorn, Nonlinear static analysis of structures with rocking columns. *Journal of structural engineering*, **136**, 532-42, 2009.

[15] I.N. Psycharis, M. Fragiadakis, I. Stefanou, Seismic reliability assessment of classical columns subjected to near‐fault ground motions. *Earthquake Engineering & Structural Dynamics*, **42**, 2061-79, 2013.

[16] S. Acikgoz, M.J. DeJong, The rocking response of large flexible structures to earthquakes. *Bulletin of earthquake engineering*, **12,** 875-908, 2014.

[17] A.A. Taflanidis, Optimal probabilistic design of seismic dampers for the protection of isolated bridges against near-fault seismic excitations. *Engineering structures*, **33**, 3496-508, 2011.

[18] A. Lamprou, G. Jia, A.A. Taflanidis, Life-cycle seismic loss estimation and global sensitivity analysis based on stochastic ground motion modeling. *Engineering structures*. **54**, 192-206, 2013.

[19] G.P. Mavroeidis, A.S. Papageorgiou, A mathematical representation of near-fault ground motions. *Bulletin of the seismological society of America*, **93**, 1099-131, 2003.

[20] R. Rupakhety, S. Sigurdsson, A. Papageorgiou, R. Sigbjörnsson, Quantification of ground-motion parameters and response spectra in the near-fault region. *Bulletin of earthquake engineering*, **9**, 893-930, 2011.

[21] The MathWorks Inc., Guide MUs. South Natick MA., 2012.

[22] B. Halldórsson, G.P. Mavroeidis, A.S. Papageorgiou, Near-fault and far-field strong ground-motion simulation for earthquake engineering applications using the specific barrier model. *Journal of structural engineering*, **137**, 433-44, 2010.

[23] D.M. Boore, Simulation of ground motion using the stochastic method. *Pure and applied geophysics*, **160**, 635-76, 2003.

[24] G.M. Atkinson, W. Silva, Stochastic modeling of California ground motions. *Bulletin of the seismological society of America*, **90**, 255-74, 2000.

[25] N. Makris, M.F. Vassiliou, Planar rocking response and stability analysis of an array of free - standing columns capped with a freely supported rigid beam. *Earthquake Engineering & Structural Dynamics*, **42**, 431-49, 2013.

[26] E. Dimitrakopoulos, A.J. Kappos, N. Makris, Dimensional analysis of yielding and pounding structures for records without distinct pulses. *Soil Dynamics and Earthquake Engineering*, **29**, 1170-80, 2009.

[27] E. Buckingham, On physically similar systems; illustrations of the use of dimensional equations. *Physical Review*, **4**, 345-76, 1914.

[28] D.B. Siano DB, Orientational analysis—a supplement to dimensional analysis—I. *Journal of The Franklin Institute*, **320**, 267-83, 1985.

[29] D. Konstantinidis, N. Makris, Experimental and analytical studies on the response of 1/4-scale models of freestanding laboratory equipment subjected to strong earthquake shaking. *Bulletin of earthquake engineering*, **8**, 1457-77, 2010.

[30] E.G. Dimitrakopoulos, T.S. Paraskeva, Dimensionless fragility curves for rocking response to near - fault excitations. *Earthquake Engineering & Structural Dynamics*, DOI:10.1002/eqe.2571, 2015.

[31] J.E. Padgett, B.G. Nielson, R. DesRoches, Selection of optimal intensity measures in probabilistic seismic demand models of highway bridge portfolios. *Earthquake Engineering & Structural Dynamics*, **37**, 711-25, 2008.

[32] C.A. Cornell, F. Jalayer, R.O. Hamburger, D.A. Foutch, Probabilistic basis for 2000 SAC federal emergency management agency steel moment frame guidelines. *Journal of structural engineering*, **128**, 526-33, 2002.